JACS
JOURNAL OF THE AMERICAN CHEMICAL SOCIETY
Article
Cite This: J. Am. Chem. Soc. 2017, 139, 15429-15436
pubs.acs.org/JACS

Highly Efficient Photocatalytic Water Splitting over Edge-Modified Phosphorene Nanoribbons

Wei Hu,*,† Lin Lin,*,‡,† Ruiqi Zhang,§ Chao Yang,*,† and Jinlong Yang*,§

†Computational Research Division, Lawrence Berkeley National Laboratory, Berkeley, California 94720, United States
‡Department of Mathematics, University of California, Berkeley, California 94720, United States
§Hefei National Laboratory for Physical Sciences at Microscale, Department of Chemical Physics, and Synergetic Innovation Center of Quantum Information and Quantum Physics, University of Science and Technology of China, Hefei, Anhui 230026, China

Supporting Information

ABSTRACT: Two-dimensional phosphorene with desirable optoelectronic properties (ideal band gap, high carrier mobility, and strong visible light absorption) is a promising metal-free photocatalyst for water splitting. However, the band edge positions of the valence band maximum (VBM) and conduction band maximum (CBM) of phosphorene are higher than the redox potentials in photocatalytic water splitting reactions. Thus, phosphorene can only be used as the photocathode for hydrogen evolution reaction as a low-efficiency visible-light-driven photocatalyst for hydrogen production in solar water splitting cells. Here, we propose a new mechanism to improve the photocatalytic efficiency of phosphorene nanoribbons (PNRs) by modifying their edges for full reactions in photocatalytic water splitting. By employing first-principles density functional theory calculations, we find that pseudohalogen (CN and OCN) passivated PNRs not only show desired VBM and CBM band edge positions induced by edge electric dipole layer, but also possess intrinsic optoelectronic properties of phosphorene, for both water oxidation and hydrogen reduction in photocatalytic water splitting without using extra energy. Furthermore, our calculations also predict that the maximum energy conversion efficiency of heterojunction solar cells consisting of different edge-modified PNRs can be as high as 20% for photocatalytic water splitting.

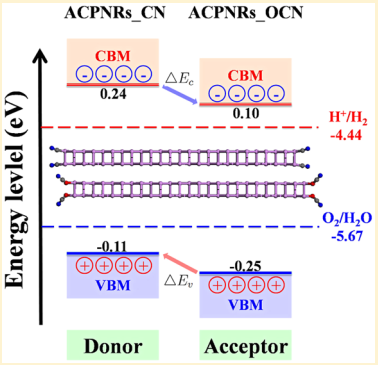

1. INTRODUCTION

Photocatalytic water splitting is an artificial photosynthesis process that uses photocatalysis in a photoelectrochemical cell to initiate the light-driven splitting of water into its elemental constituents, H_2 and O_2.[1−3] Theoretically, only sunlight, water, and a photocatalyst are required for water splitting reactions. The mechanism of photocatalytic water splitting involves electrons being excited from the valence band maximum (VBM) to the conduction band maximum (CBM) of the semiconductor photocatalyst by the absorbed sunlight, forming the electron−hole pairs; thus, the photogenerated electrons and holes can participate in the hydrogen evolution reaction (HER) H^+/H_2 ($2H^+ + 2e^- \rightleftharpoons H_2$) and oxygen evolution reaction (OER) O_2/H_2O ($O_2 + 4H^+ + 4e^- \rightleftharpoons 2H_2O$), respectively. However, there are several crucial factors for such a promising semiconductor photocatalyst for absorbing sunlight and driving two water splitting reactions, such as a small direct band gap of roughly 1.2−1.6 eV to absorb wide range sunlight[4] and a high carrier mobility to facilitate efficient transport. In particular, the redox potentials of photocatalytic water splitting reactions should be located inside the energy gap of semiconductor photocatalyst as shown in Figure 1, which means that the VBM energy level should be more negative than the oxidation potential of OER (O_2/H_2O) but the CBM energy level should be more positive than the reduction potential of HER (H^+/H_2) in photocatalytic water splitting reactions, respectively. Furthermore, if the band edge positions of VBM and CBM in semiconductor photocatalyst are located closer to the redox potentials of photocatalytic water splitting reactions, the photocatalytic efficiency would be higher in full water splitting reactions. Most of such semiconductor photocatalysts for water splitting have been discovered in transition metal oxides, sulfides, and nitrides,[5] such as titanium dioxide (TiO_2).[6−8]

Recently, two-dimensional (2D) monolayer semiconductors[9−11] have been also proposed as potential candidates to be used in photocatalytic water splitting,[12] such as graphitic carbon nitride ($g\text{-}C_3N_4$)[13−15] and molybdenum disulfide (MoS_2).[16−18] Such 2D semiconductor photocatalysts exhibit two desirable advantages that can be utilized to enhance the photocatalytic efficiency of water splitting.[12] One is that 2D materials have large photoreactive contact area for light absorption and photocatalytic reactions. Moreover, the small distance between photogenerated electrons and holes to allows them to reach the water interface more rapidly for photocatalytic reactions. However, $g\text{-}C_3N_4$ and MoS_2 have wide band gaps (2−3 eV),[19] similar to most other 3D semiconductor photocatalysts. This shortcoming limits the light absorption in the ultraviolet region for these semiconductor photocatalysts. Furthermore, the activity of HER or OER remains poor in such semi-

Received: August 9, 2017
Published: October 13, 2017

DOI: 10.1021/jacs.7b08474
J. Am. Chem. Soc. 2017, 139, 15429−15436

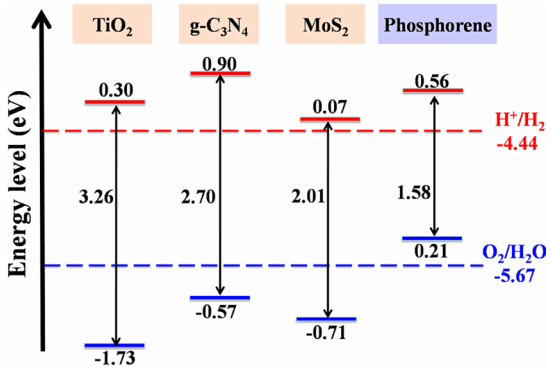

Figure 1. Schematic illustration of band edge positions of TiO_2, g-C_3N_4, MoS_2, and phosphorene as water splitting photocatalysts. The reduction potential of H^+/H_2 and the oxidation potential of O_2/H_2O are marked by the dotted red and blue lines, respectively. The CBM and VBM band edge positions are marked by the solid red and blue lines, respectively. The values of the CBM and VBM energy level relative to the redox potentials are marked close to corresponding CBM and VBM band edge positions. The energy gaps of semiconductor photocatalysts are marked by the black arrows. All the energy levels are referenced to the vacuum level, which is set to zero.

conductor photocatalysts, because their band edge positions of VBM or CBM are far away from the redox potentials of photocatalytic water splitting reactions. For example, TiO_2 and MoS_2 show high photocatalytic efficiency for HER, because their CBM energy levels are located close (0.1−0.3 eV) to the reduction potential of HER. But their VBM energy levels are located much lower (1.73−0.71 eV) than the oxidation potential of OER. On the other hand, as the hot star in 2D materials, graphene[20−22] has a high carrier mobility of up to 10^6 $cm^2/(V{\cdot}s)$ but lacks an intrinsic band gap; thus it can only be used as a cocatalyst in combination with other 2D materials in heterostructures to improve the photocatalytic efficiency in water splitting.[23]

Phosphorene is an interesting 2D elemental material[24−27] that has been isolated experimentally through mechanical exfoliation from bulk black phosphorus. Phosphorene exhibits some remarkable optoelectronic properties[28] that are superior to graphene, g-C_3N_4, and MoS_2. For example, phosphorene is a direct semiconductor with a high hole mobility[24] of 10^5 $cm^2/(V{\cdot}s)$. When placed in nanoelectronics,[25] it exhibits drain current modulation of up to 10^5. It is the building block for black phosphorus quantum dots[27] that have been used to fabricate a flexible memory device with a high on−off current ratio of 6×10^4 and good stability. Furthermore, phosphorene possesses a thickness-dependent direct bandgap[24] in a wide range of 0.3 eV (bulk) to 1.6 eV (monolayer), which bridges the gap between graphene and MoS_2 for new optoelectronic devices. The thickness dependency of the bandgap allows one to tune the bandgap of phosphorene based materials and enhance light absorption by varying the number of layers. Compared to graphene,[29] g-C_3N_4,[30] and MoS_2,[31] phosphorene shows superior optical properties for strong optical absorption in the near-infrared region of sunlight.[32] Therefore, phosphorene has been considered to be a promising metal-free photocatalyst for solar water splitting cells.[33]

However, the VBM and CBM band edge positions of phosphorene are both more positive than the oxidation potential of O_2/H_2O and the reduction potential of H^+/H_2, respectively. Furthermore, the CBM energy level is much higher (0.56 eV) than the reduction potential of H^+/H_2 (Figure 1). Thus, phosphorene can only be used as the photocathode for HER as a low-efficiency visible-light-driven photocatalyst for hydrogen production in solar water splitting cells.[33] There are some external conditions and experimental techniques, such as electrical bias,[34,35] mechanical strain,[36] defect or dopant doping[37,38] and pH,[39,40] which can be used to tune the band edge positions of semiconductor photocatalysts, but such methods also affect their desired optoelectronic properties for photocatalytic water splitting. Recently, Sa et al.[41] predicted that strain-engineered phosphorene can be an effective water splitting photocatalyst at a given pH of 8 by using first-principles density functional theory (DFT) calculations. Furthermore, several phosphorene based heterostructures have also been proposed experimentally and theoretically as photocatalysts for water splitting, such phosphorene/TiO_2[42,43] and phosphorene/MoS_2.[44] However, most of these methods require extra energy input for maintenance or are difficult to realize in experiments for practical industrial applications in solar water splitting cells.[1]

In this paper, we propose a new mechanism to use edge-modified phosphorene nanoribbons (PNRs) directly as highly efficient photocatalysts for water splitting. By using density functional theory calculations, we find that pseudohalogen passivated PNRs show desired VBM and CBM band edge positions induced by edge electric dipole layer, but with the intrinsic optoelectronic properties of phosphorene preserved, for both water oxidation and hydrogen reduction in photocatalytic water splitting, without extra energy being necessary.

2. THEORETICAL MODELS AND COMPUTATIONAL METHODS

When phosphorene is cut into nanoribbons, edge passivation is required to stabilize the PNRs.[44,45] PNRs have already been experimentally synthesized for nanoelectronics.[46,47] Different types of chemical atoms or groups can be used to passivate the edges of PNRs. Notice that the stability and optoelectronic properties of PNRs depend sensitively on the ribbon width, edge passivated atoms or groups, and edge shaped types (armchair or zigzag).[44] Some examples of armchair and zigzag PNRs (ACPNRs and ZZPNRs) passivated by nitrile (CN) functional group (ACPNRs_CN and ZZPNRs_CN) are shown in Figure 2. Here, the ACPNRs passivated by nitrile (CN) and cyanate (OCN) functional groups in a ribbon width of 4 are denoted as ACPNR4_CN and ACPNR4_OCN, respectively.

Notice that edge passivation can introduce polar covalent bonds around the edges of the PNRs.[48] These covalent bonds create edge dipole layers that produce constant electric potential jumps, $\phi(\vec{r})$ in the form of $p/4\sqrt{2}\pi\varepsilon|\vec{r}| < |\phi(\vec{r})| < p/4\pi\varepsilon|\vec{r}|$ inside PNRs, where $\vec{r}$ is the distance close to the edges and p represents the electric dipole moment per unit edge length at the edges of PNRs. Such a potential jump shifts all single particle energy levels down, including the CBM and VBM energy levels. Therefore, polar covalent bonds in the form of P^+-X^- (X is an atom or a chemical group) can be used to shift downward the CBM and VBM energy levels of phosphorene, and such a strong edge decoration effect on the CBM and VBM levels of edge-modified PNRs makes it possible to design efficient photocatalysts that are suitable for both HER and OER in photocatalytic water splitting.

We use the first-principles density functional theory (DFT) calculations implemented in the VASP (Vienna Ab initio Simulation Package) package.[49] We choose the generalized gradient approximation of Perdew, Burke, and Ernzerhof (GGA-PBE)[50] as the exchange-correlation functional to study the geometric structures of phosphorene and PNRs. However, because semilocal GGA-PBE based DFT calculations are less reliable in predicting electronic properties of semiconductors, the screened hybrid HSE06 functional[51] is also used to compute the optoelectronic properties. We set the energy cutoff to

DOI: 10.1021/jacs.7b08474
J. Am. Chem. Soc. 2017, 139, 15429−15436

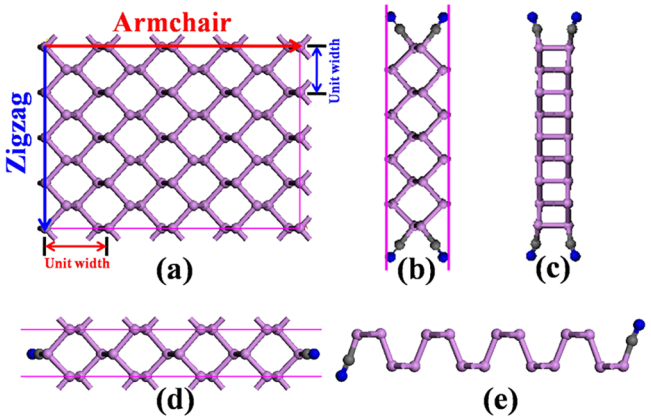

Figure 2. Geometric structures of pristine phosphorene and edge-modified PNRs: (a) phosphorene in a 4 × 4 supercell; (b, c) top and side views of ACPNRs passivated by nitrile (CN) functional group in ribbon width of 4 (ACPNR4_CN); (d, e) top and side views of ZZPNRs by nitrile (CN) functional group in ribbon width of 4 (ZZPNR4_CN). Two types of edges, armchair and zigzag, are highlighted in the inset. The unit widths of armchair and zigzag edges are defined in the inset. The violet, gray, blue, and red balls denote silicon and phosphorus, carbon, nitrogen, and oxygen atoms, respectively.

500 eV. The surface Brillouin zone is sampled with a 1 × 1 × 8 uniform mesh for PNRs. All the geometry structures are fully relaxed by using a nonlinear conjugate gradient (CG) algorithm until total energy and atomic forces are converged within error tolerances of 10^{-5} eV and 0.01 eV/Å, respectively.

We use the density functional perturbation theory[52] implemented in VASP to compute the optical properties of edge-modified PNRs. We adopt a fine 1 × 1 × 12 uniform mesh for the surface Brillouin zone and a large number of empty conduction band states (two times the number of valence band) and frequency grid points (2000) for computing optical absorption spectra of phosphorene[32] and PNRs.

Ab-initio molecular dynamics (AIMD) simulations are performed to study the stability of edge-modified PNRs. The simulations are performed for about 10.0 ps with a time step of 1.0 fs at temperatures of T = 300, 600, and 800 K controlled by a Nose−Hoover thermostat.[53,54]

3. RESULTS AND DISCUSSION

In principle, atoms or chemical groups that have larger chemical electronegativity than the phosphorus (P) atom can be used to passivate the edges of PNRs and form polar covalent bonds in the form of P^+-X^- (X is an atom or a chemical group). The electronegativity of the functional atoms and groups has a strong effect on the band offset shift of phosphorene, because functional atoms and groups with large electronegativity can introduce polar covalent bonds with large electric dipole moments. In experiments, the halogen atoms (X = F, Cl, and Br), hydroxyl (X = OH) and pseudohalogen chemical groups (X = CN, OCN, and SCN) are widely used for surface or edge passivation. Here, we find that PNRs passivated by pseudohalogen chemical groups (CN and OCN) show desired VBM and CBM band edge positions for both water oxidation and hydrogen reduction in photocatalytic water splitting. In this section, we check the effects of edge-passivated chemical groups (CN and OCN), the edge-shape types (armchair or zigzag), and ribbon width on the optoelectronic properties of edge-modified PNRs. Other PNRs with X = H, F, Cl, and OH do not have desired VBM and CBM band edge positions for either water oxidation or hydrogen reduction in photocatalytic water splitting, because effective electric dipole moments introduced by these edge-passivated chemical groups are not enough to shift downward the CBM and VBM energy levels of phosphorene. We summarize the electronic structures (VBM and CBM band positions and energy gaps) of these low-efficient PNR photocatalysts in Table S1 in the Supporting Information.

3.1. Electronic Structures of PNRs. We first study the electronic structures of edge-modified PNRs with small ribbon width. Figure 3 shows electronic band structures of

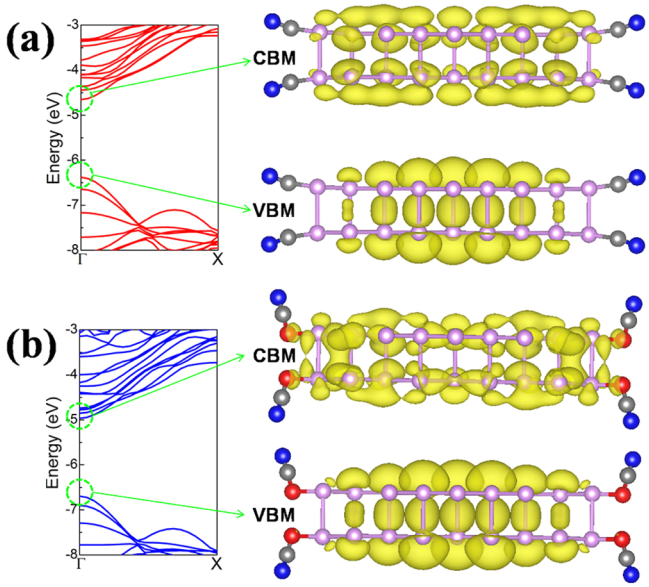

Figure 3. Electronic band structures of small scale ACPNRs with different edge-passivated types (CN and OCN) in ribbon width of 4: (a) ACPNR4_CN and (b) ACPNR4_OCN. The VBM and CBM levels are marked by green dotted circles and corresponding states are shown in the right side of figure. All the energy levels are referenced to the vacuum level, which is set to zero.

ACPNR4_CN and ACPNR4_OCN. Both of them have direct band gaps of about 1.73 eV, and their VBM and CBM band edge positions are both located at the gamma point with strong optical absorption under sunlight. Furthermore, we find that the VBM and CBM states of ACPNR4_CN and ACPNR4_OCN are only dominated by p-orbitals of P atoms (Figure S1 and S2 in Supporting Information) and show similar characteristics to pristine phosphorene without containing any edge states; this is different from other low dimensional nanoribbons, such as graphene nanoribbons[55−59] and boron nitride nanoribbons,[60−62] which show reduced energy gaps due to the edge states dominated in the VBM and CBM states. That is why they have similar band gap values even though they are edge-passivated with different types of chemical groups when in the same ribbon width. Therefore, the band gaps of edge-modified ACPNRs and ZZPNRs are mainly affected by the ribbon widths due to the well-known quantum confinement effect (QCE) in nanomaterials.[63−65]

Figure 4 shows that the band gaps of edge-modified PNRs decrease as the ribbon widths increase. We find that the band gap values of ZZPNRs decrease more quickly than those of ACPNRS due to different edge-shaped types. For large-scale ACPNRs, when the ribbon widths increase to 12, the band gap values (1.59 eV) of ACPNR12_CN and ACPNR12_OCN are almost converged and close to that (1.58 eV)[24] of pristine

DOI: 10.1021/jacs.7b08474
J. Am. Chem. Soc. 2017, 139, 15429−15436

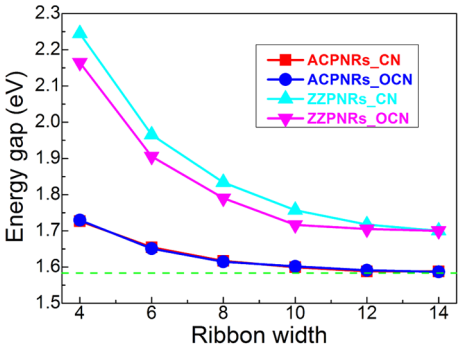

Figure 4. Energy gaps of PNRs in different edge-shaped types (armchair and zigzag), edge-passivated types (CN and OCN), and ribbon width. The energy gap of pristine phosphorene is marked by green dotted lines.

phosphorene as shown in Figure 5. But the band gaps of ZZPNR12_CN and ZZPNR12_OCN are slightly larger (about 1.7 eV) than that of pristine phosphorene.

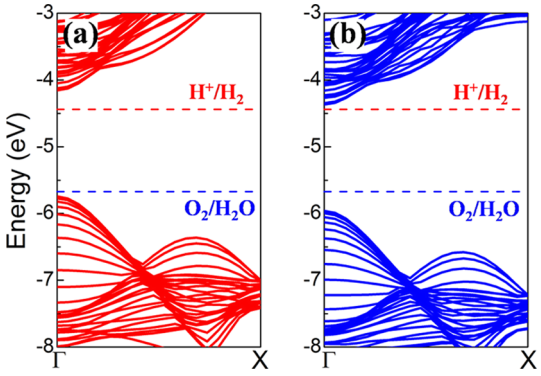

Figure 5. Electronic band structures of large scale ACPNRs with different edge-passivated types (CN and OCN) in ribbon width of 12: (a) ACPNR12_CN and (b) ACPNR12_OCN. The reduction potential of H^+/H_2 and the oxidation potential of O_2/H_2O are marked by the dotted red and blue lines, respectively. All the energy levels are referenced to the vacuum level, which is set to zero.

Although the band gaps of large scale PNRs appear to be insensitive to the types of edge passivation, their VBM and CBM energy levels are strongly affected by the edge-modified decoration as shown in Figure 6. Interestingly, we find that CN and OCN groups of ACPNRs and ZZPNRs in edge passivation can shift the VBM and CBM energies down with respect to pristine phosphorene. In particular, large scale ACPNRs and ZZPNRs show desired VBM and CBM band edge positions for both water oxidation and hydrogen reduction in photocatalytic water splitting. This observation is consistent with our theoretical models based on the edge dipole layer. Taking large scale ACPNR12_CN and ACPNR12_OCN as examples, the redox potentials of photocatalytic water splitting reactions now are located inside the energy gap of PNRs. In detail, the P atoms near the edges of these systems lose 0.44 and 0.58 electrons, respectively. These electrons are transferred into passivated chemical groups (CN and OCN) and cause electric potential energy to jump about −1.3 and −1.5 eV (Table S2 in the Supporting Information) close to the edges (about 1 Å) in ACPNR12_CN and ACPNR12_OCN, respectively. The DFT calculations show that the VBM energy levels of ACPNR12_CN and ACPNR12_OCN are, respectively, 0.11

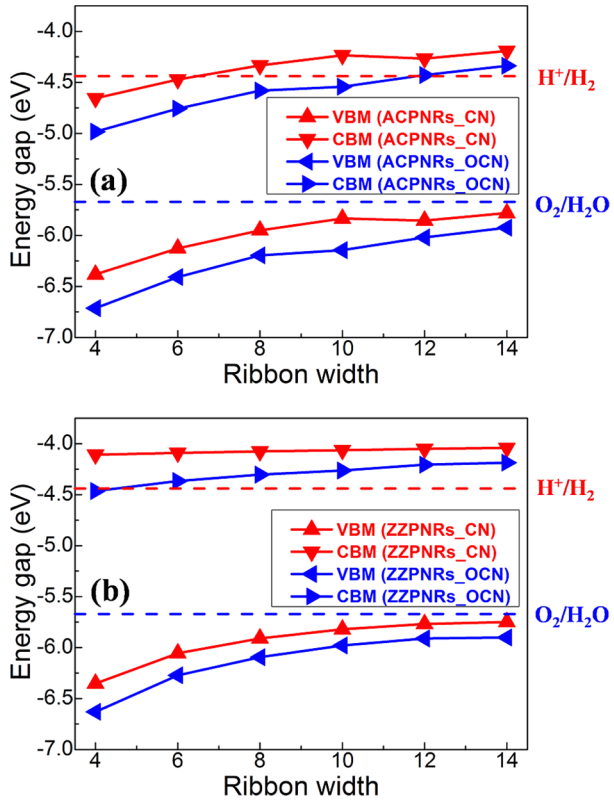

Figure 6. Band edge positions of the valence band maximum (VBM) and conduction band maximum (CBM) of PNRs in different edge-shaped types (armchair and zigzag), edge-passivated types (CN and OCN), and ribbon width: (a) ACPNRs and (b) ZZPNRs. The reduction potential of H^+/H_2 and the oxidation potential of O_2/H_2O are marked by the dotted red and blue lines, respectively. All the energy levels are referenced to the vacuum level, which is set to zero.

and 0.25 eV lower than the oxidation potential of O_2/H_2O and their CBM energy level are, respectively, 0.24 and 0.10 eV higher than the reduction potential of H^+/H_2. Therefore, such edge-modified PNRs can be used as highly efficient photocatalysts for full water splitting reactions. Notice that the functional groups are the key factor for PNRs as promising photocatalysts. The effects of nanoribbon type and nanoribbon width on electronic structures are weakened and become negligible as the system size increases, although ACPNRs show higher linear density of edges with larger dipole moments per edge length compared to the case of ZZPNRs (Table S2 in Supporting Information).

3.2. Solar Water Splitting Cells of PNR Heterobilayers.

In this section, we propose efficient solar water splitting cells by using edge-modified PNR heterojunctions. We design a PNR heterobilayer consisting of two types of edge-modified PNRs. The heterobilayer serves as a type-II donor−acceptor interface band heterojunction,[66] as illustrated in Figure 7. This type of heterojunction can promote carrier (electron and hole) transfer and separation at the heterobilayer interface due to the built-in potential induced by the edge dipole layers inside PNRs. Such an induced potential is likely to localize VBM and CBM states within distinctive donor and acceptor regions. It is the localization of the VBM and CBM states that ultimately leads to enhanced charge separation and enables carriers to be easily collected. These properties can lead to improved carrier lifetime when the heterojunction is used in solar cells.[67]

DOI: 10.1021/jacs.7b08474
J. Am. Chem. Soc. 2017, 139, 15429−15436

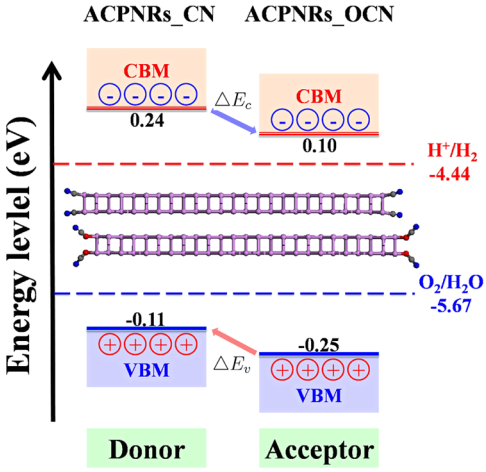

Figure 7. Schematic illustration of type-II donor–acceptor band alignments for the carrier transfer and separation in hybrid edge-modified PNR heterobilayers as solar water splitting cells. ΔE_c and ΔE_v represent the conduction and valence band offsets, respectively. The reduction potential of H^+/H_2 and the oxidation potential of O_2/H_2O are marked by the dotted red and blue lines, respectively. The CBM and VBM band edge positions are marked by the solid red and blue lines, respectively. The values of the CBM and VBM energy level relative to the redox potentials are marked close to corresponding CBM and VBM band edge positions. All the energy levels are referenced to the vacuum level, which is set to zero.

Taking hybrid ACPNR12_CN/ACPNR12_OCN heterobilayer as examples, Figure 8 shows the total density of states

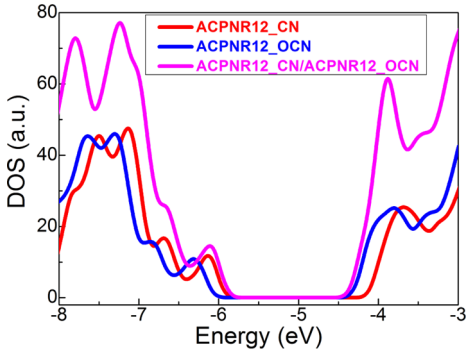

Figure 8. Total density of states (TDOS) of PNRs with different edge-passivated types (ACPNR12_CN and ACPNR12_OCN) and corresponding PNRs heterobilayer (ACPNR12_CN/ACPNR12_OCN). All the energy levels are referenced to the vacuum level, which is set to zero.

(TDOS) of ACPNR12_CN and ACPNR12_OCN as well as corresponding hybrid ACPNR12_CN/ACPNR12_OCN heterobilayer. We find that such heterobilayers have a reduced band gap compared to isolated ACPNR12_CN and ACPNR12_OCN. Furthermore, the VBM states are located at the ACPNR12_CN region where OER occurs but the CBM states are located at another ACPNR12_OCN region for HER, which is consistent with our theoretical models as illustrated in Figure 7.

Such reduced band gap in hybrid PNR heterobilayers can increase the absorption range of sunlight. Furthermore, interlayer interaction[30] and charge transfer[68] at the heterobilayer interface can induce new optical transitions that result from the overlap of electronic states and enhance the optical absorption intensity in hybrid PNR heterobilayers. Figure 9 shows that hybrid ACPNR12_CN/ACPNR12_OCN heterobilayer shows wider absorption range and stronger optical absorption compared to isolated ACPNR12_CN and ACPNR12_OCN.

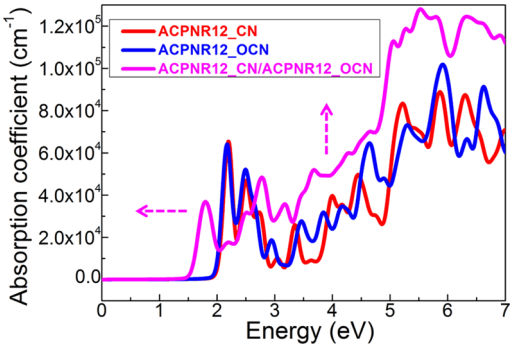

Figure 9. Absorption coefficient of PNRs with different edge-passivated types (ACPNR12_CN and ACPNR12_OCN) and corresponding PNR heterobilayer (ACPNR12_CN/ACPNR12_OCN). The wider absorption range and stronger optical absorption of PNR heterobilayer are marked by dotted pink arrows.

For realistic optoelectronic devices, the exciton effect in 2D semiconductors can induce a red shift of absorption spectra and affect the light absorption efficiency for 2D semiconductors, although such exciton effect in phosphorene does not qualitatively affect our proposed edge-modified heterojunction model for photocatalytic water splitting. The GW-BSE calculations[69] have shown that the electron–hole binding energy of monolayer phosphorene is about 0.48 eV, which is the smallest exciton binding energy among popular 2D semiconductors due to the small band gap of phosphorene.[70] Notice that bilayer phosphorene only show a small electron–hole binding energy of about 0.22 eV, similar to the case in PNRs based on heterostructures. Furthermore, additional substrates interfacing with phosphorene can not only effectively reduce the electron–hole binding energy of phosphorene monolayer (0.14 eV) and bilayer (0.11 eV) due to environmental screening effect but also avoid the degradation of phosphorene under ambient conditions.

From a practical perspective, the quality of heterojunction solar cells depends on the power conversion efficiency (PCE) defined as[71]

$$\eta = \frac{0.65(E_g - \Delta E_c - 0.3)\int_{E_g}^{\infty} \frac{P(\hbar\varpi)}{\hbar\varpi}\, d(\hbar\varpi)}{\int_0^{\infty} P(\hbar\varpi)\, d(\hbar\varpi)}$$

where 0.65 is the band-fill factor, $P(\hbar\varpi)$ is the AM1.5 solar energy flux at the photon energy $\hbar\varpi$, E_g is the bandgap of the donor, ΔE_c is the conduction band offsets, and the $(E_g - \Delta E_c - 0.3)$ term is an estimation of the maximum open circuit voltage.

The maximum PCE depends critically on the interface band alignment between donor and acceptor materials.[71] For large-scale hybrid heterobilayers consisting of two different edge-modified PNRs, such ACPNR12_CN/ACPNR12_OCN, the bandgap values E_g of donor and acceptor monolayers are similar (1.59 eV), which are close to that (1.58 eV) of pristine phosphorene.[44] This gap value is very suitable for the absorption of the solar spectrum[71] and can be tuned by changing the number of layers in multilayer phosphorene.[24]

DOI: 10.1021/jacs.7b08474
J. Am. Chem. Soc. 2017, 139, 15429–15436

The conduction band offset ΔE_c between ACPNR12_CN and ACPNR12_OCN is ΔE_c = 0.15 eV for a hybrid ACPNR12_CN/ACPNR12_OCN heterobilayer, which is close to the optimal value of conduction band offset to achieve high PCE in heterojunction solar cells.[34] Therefore, large-scale PNR heterobilayers can achieve PCE as high as 20%. These values are comparable to that of recently proposed heterobilayers, such as α-AlP/GaN (22%),[72] edge-modified phosphorene nanoflakes (20%),[48] g-SiC_2/g-ZnO (20%),[73] PCBM/CBN (20%),[71] and phosphorene/MoS_2 (18%),[34] for highly efficient solar cells.

3.3. Stability. The stability of edge-modified PNRs under ambient conditions is crucial in solar water splitting cells.[74] Here, we study the thermal and dynamic stabilities of edge-modified PNRs by computing the edge formation energy (Table S3 in the Supporting Information) and performing AIMD simulations (Figures S3 and S4 in the Supporting Information). Notice that PNRs have already been successfully synthesized in experiments for nanoelectronics.[46,47] Here, we find that most halogen atoms (X = F, Cl and Br) and pseudohalogen chemical groups (X = CN and OCN) are stable even at high temperature of T = 800 K as edge passivation elements for PNRs, except for the SCN chemical group, which is easy to dissociate when bonded with P atom in PNRs. The OCN passivated PNRs (both ACPNRs and ZZPNRs) show small edge formation energies of less than 0.2 eV per edge, which are easily fabricated in experiments, similar to cases of H passivated PNRs.[44] But the CN passivated PNRs require relatively large edge formation energies of about 1.5 eV per edge. We also check the stability of PNRs in aqueous environment by using AIMD simulations and find that edge-modified PNRs remain stable in liquid water at high temperature, similar to the case of phosphorene in liquid water.[41] Therefore, our proposed highly efficient heterojunction photocatalyst for water splitting can survive at high temperature in experiments.

However, phosphorene is sensitive to oxygen molecules[75] and easily degrades in ambient conditions.[76] Experimentally, some techniques, such as liquid exfoliation[77] and Al_2O_3 coating passivation,[78] have been recently reported to produce air-stable phosphorene for photocatalytic applications. Furthermore, hybrid phosphorene/TiO_2 photocatalysts, which have recently been synthesized in experiments,[42,43] show high stability in ambient conditions and improved photocatalytic performance under light irradiation. Therefore, additional substrates interfacing with PNRs can not only effectively reduce the electron−hole binding energy of PNRs due to environmental screening effect[69] but also avoid the degradation of phosphorene under ambient conditions and improve the photocatalytic performance as highly efficient photocatalysts[79] used in water splitting for clean and renewable hydrogen energy.

4. CONCLUSION

In summary, we propose a new mechanism to use edge-modified phosphorene nanoribbons (PNRs) directly as highly efficient photocatalysts for full reactions of both water oxidation and hydrogen reduction in water splitting. By using density functional theory calculations, we find that pseudohalogen (CN and OCN) passivated PNRs show desired VBM and CBM band edge positions induced by edge electric dipole layer, but with the intrinsic optoelectronic properties of phosphorene preserved, for both water oxidation and hydrogen reduction in photocatalytic water splitting, without requiring extra energy. Furthermore, our calculations also predict that the maximum energy conversion efficiency of the heterojunctions consisting of different edge-modified PNRs can be as high as 20% for solar water splitting cells.

■ ASSOCIATED CONTENT

Supporting Information

This Supporting Information is available free of charge via the Internet at The Supporting Information is available free of charge on the ACS Publications website at DOI: 10.1021/jacs.7b08474.

VBM and CBM band positions, energy gaps, edge formation energy, charge transfer and potential energy jump induced by edge dipole layer, projected density of state (PDOS), and AIMD simulations of ACPNR4_CN and ACPNR4_OCN at T = 300 and 800 K (PDF)

■ AUTHOR INFORMATION

Corresponding Authors

*whu@lbl.gov
*linlin@math.berkeley.edu
*cyang@lbl.gov
*jlyang@ustc.edu.cn

ORCID

Wei Hu: 0000-0001-9629-2121
Lin Lin: 0000-0001-6860-9566
Ruiqi Zhang: 0000-0002-7820-6020
Jinlong Yang: 0000-0002-5651-5340

Notes

The authors declare no competing financial interest.

■ ACKNOWLEDGMENTS

This work is partially supported by the Scientific Discovery through Advanced Computing (SciDAC) Program funded by U.S. Department of Energy, Office of Science, Advanced Scientific Computing Research and Basic Energy Sciences (W.H., L.L. and C.Y.), and by the Center for Applied Mathematics for Energy Research Applications (CAMERA), which is a partnership between Basic Energy Sciences and Advanced Scientific Computing Research at the U.S Department of Energy (L.L. and C.Y.). This work is also partially supported by the National Key Research & Development Program of China (Grant No. 2016YFA0200604) and the National Natural Science Foundation of China (NSFC) (Grant No. 21688102). We thank the National Energy Research Scientific Computing (NERSC) center, and the USTCSCC, SC-CAS, Tianjin, and Shanghai Supercomputer Centers for the computational resources. We would like to thank Prof. Yuan Ping (UC Santa Cruz) and Dr. Jun Dai (University of Nebraska-Lincoln) for helpful discussions.

■ REFERENCES

(1) Walter, M. G.; Warren, E. L.; McKone, J. R.; Boettcher, S. W.; Mi, Q.; Santori, E. A.; Lewis, N. S. *Chem. Rev.* **2010**, *110*, 6446−6473.
(2) Chen, X.; Shen, S.; Guo, L.; Mao, S. S. *Chem. Rev.* **2010**, *110*, 6503−6570.
(3) Qu, Y.; Duan, X. *Chem. Soc. Rev.* **2013**, *42*, 2568−2580.
(4) Shockley, W.; Queisser, H. J. *J. Appl. Phys.* **1961**, *32*, 510−519.
(5) McCrory, C. C. L.; Jung, S.; Ferrer, I. M.; Chatman, S. M.; Peters, J. C.; Jaramillo, T. F. *J. Am. Chem. Soc.* **2015**, *137*, 4347−4357.
(6) Fujishima, A.; Honda, K. *Nature* **1972**, *238*, 37−38.

(7) Khan, S. U. M.; Al-Shahry, M.; Ingler, W. B., Jr. *Science* **2002**, *297*, 2243−2245.
(8) Ni, M.; Leung, M. K.; Leung, D. Y. C.; Sumathy, K. *Renewable Sustainable Energy Rev.* **2007**, *11*, 401−425.
(9) Novoselov, K. S.; Jiang, D.; Schedin, F.; Booth, T. J.; Khotkevich, V. V.; Morozov, S. V.; Geim, A. K. *Proc. Natl. Acad. Sci. U. S. A.* **2005**, *102*, 10451.
(10) Osada, M.; Sasaki, T. *Adv. Mater.* **2012**, *24*, 210.
(11) Xu, M.; Liang, T.; Shi, M.; Chen, H. *Chem. Rev.* **2013**, *113*, 3766.
(12) Singh, A. K.; Mathew, K.; Zhuang, H. L.; Hennig, R. G. *J. Phys. Chem. Lett.* **2015**, *6*, 1087−1098.
(13) Wang, X.; Maeda, K.; Thomas, A.; Takanabe, K.; Xin, G.; Carlsson, J. M.; Domen, K.; Antonietti, M. *Nat. Mater.* **2009**, *8*, 76−80.
(14) Wang, X.; Maeda, K.; Chen, X.; Takanabe, K.; Domen, K.; Hou, Y.; Fu, X.; Antonietti, M. *J. Am. Chem. Soc.* **2009**, *131*, 1680−1681.
(15) Cao, S.; Yu, J. *J. Phys. Chem. Lett.* **2014**, *5*, 2101−2107.
(16) Hinnemann, B.; Moses, P. G.; Bonde, J.; Jørgensen, K. P.; Nielsen, J. H.; Horch, S.; Chorkendorff, I.; Nørskov, J. K. *J. Am. Chem. Soc.* **2005**, *127*, 5308−5309.
(17) Li, Y.; Li, Y.-L.; Araujo, C. M.; Luo, W.; Ahuja, R. *Catal. Sci. Technol.* **2013**, *3*, 2214−2220.
(18) Joshi, R. K.; Shukla, S.; Saxena, S.; Lee, G.-H.; Sahajwalla, V.; Alwarappan, S. *AIP Adv.* **2016**, *6*, 015315.
(19) Wang, J.; Guan, Z.; Huang, J.; Li, Q.; Yang, J. *J. Mater. Chem. A* **2014**, *2*, 7960−7966.
(20) Novoselov, K. S.; Geim, A. K.; Morozov, S. V.; Jiang, D.; Zhang, Y.; Dubonos, S. V.; Grigorieva, I. V.; Firsov, A. A. *Science* **2004**, *306*, 666−669.
(21) Geim, A. K.; Novoselov, K. S. *Nat. Mater.* **2007**, *6*, 183−191.
(22) Castro Neto, A. H. C.; Guinea, F.; Peres, N. M. R.; Novoselov, K. S.; Geim, A. K. *Rev. Mod. Phys.* **2009**, *81*, 109.
(23) Bernardi, M.; Palummo, M.; Grossman, J. C. *Nano Lett.* **2013**, *13*, 3664−3670.
(24) Liu, H.; Neal, A. T.; Zhu, Z.; Luo, Z.; Xu, X.; Tománek, D.; Ye, P. D. *ACS Nano* **2014**, *8*, 4033−4041.
(25) Li, L.; Yu, Y.; Ye, G.; Ge, Q.; Ou, X.; Wu, H.; Feng, D.; Chen, X.; Zhang, Y. *Nat. Nanotechnol.* **2014**, *9*, 372−377.
(26) Das, S.; Zhang, W.; Demarteau, M.; Hoffmann, A.; Dubey, M.; Roelofs, A. *Nano Lett.* **2014**, *14*, 5733−5739.
(27) Zhang, X.; Xie, H.; Liu, Z.; Tan, C.; Luo, Z.; Li, H.; Lin, J.; Sun, L.; Chen, W.; Xu, Z.; Xie, L.; Huang, W.; Zhang, H. *Angew. Chem., Int. Ed.* **2015**, *54*, 3653−3657.
(28) Kou, L.; Chen, C.; Smith, S. C. *J. Phys. Chem. Lett.* **2015**, *6*, 2794−2805.
(29) Bonaccorso, F.; Sun, Z.; Hasan, T.; Ferrari, A. C. *Nat. Photonics* **2010**, *4*, 611−622.
(30) Wu, F.; Liu, Y.; Yu, G.; Shen, D.; Wang, Y.; Kan, E. *J. Phys. Chem. Lett.* **2012**, *3*, 3330−3334.
(31) Splendiani, A.; Sun, L.; Zhang, Y.; Li, T.; Kim, J.; Chim, C.-Y.; Galli, G.; Wang, F. *Nano Lett.* **2010**, *10*, 1271−1275.
(32) Qiao, J.; Kong, X.; Hu, Z.-X.; Yang, F.; Ji, W. *Nat. Commun.* **2014**, *5*, 4475.
(33) Rahman, M. Z.; Kwong, C. W.; Davey, K.; Qiao, S. Z. *Energy Environ. Sci.* **2016**, *9*, 709−728.
(34) Dai, J.; Zeng, X. C. *J. Phys. Chem. Lett.* **2014**, *5*, 1289−1293.
(35) Padilha, J. E.; Fazzio, A.; da Silva, A. J. R. *Phys. Rev. Lett.* **2015**, *114*, 066803.
(36) Peng, X.; Wei, Q.; Copple, A. *Phys. Rev. B: Condens. Matter Mater. Phys.* **2014**, *90*, 085402.
(37) Hu, W.; Yang, J. *J. Phys. Chem. C* **2015**, *119*, 20474−20480.
(38) Kistanov, A. A.; Cai, Y.; Zhou, K.; Dmitriev, S. V.; Zhang, Y.-W. *2D Mater.* **2017**, *4*, 015010.
(39) Chakrapani, V.; Angus, J. C.; Anderson, A. B.; Wolter, S. D.; Stoner, B. R.; Sumanasekera, G. U. *Science* **2007**, *318*, 1424−1430.
(40) Chen, S.; Wang, L.-W. *Chem. Mater.* **2012**, *24*, 3659−3666.
(41) Sa, B.; Li, Y.-L.; Qi, J.; Ahuja, R.; Sun, Z. *J. Phys. Chem. C* **2014**, *118*, 26560−26568.
(42) Uk Lee, H.; Lee, S. C.; Won, J.; Son, B.-C.; Choi, S.; Kim, Y.; Park, S. Y.; Kim, H.-S.; Lee, Y.-C.; Lee, J. *Sci. Rep.* **2015**, *5*, 8691.
(43) Zhou, L.; Zhang, J.; Zhuo, Z.; Kou, L.; Ma, W.; Shao, B.; Du, A.; Meng, S.; Frauenheim, T. *J. Phys. Chem. Lett.* **2016**, *7*, 1880−1887.
(44) Guo, H.; Lu, N.; Dai, J.; Wu, X.; Zeng, X. C. *J. Phys. Chem. C* **2014**, *118*, 14051−14059.
(45) Hu, W.; Lin, L.; Yang, C. *Phys. Chem. Chem. Phys.* **2015**, *17*, 31397−31404.
(46) Zhu, W.; Yogeesh, M. N.; Yang, S.; Aldave, S. H.; Kim, J.-S.; Sonde, S.; Tao, L.; Lu, N.; Akinwande, D. *Nano Lett.* **2015**, *15*, 1883−1890.
(47) Masih Das, P.; Danda, G.; Cupo, A.; Parkin, W. M.; Liang, L.; Kharche, N.; Ling, X.; Huang, S.; Dresselhaus, M. S.; Meunier, V.; Drndić, M. *ACS Nano* **2016**, *10*, 5687−5695.
(48) Hu, W.; Lin, L.; Yang, C.; Dai, J.; Yang, J. *Nano Lett.* **2016**, *16*, 1675−1682.
(49) Kresse, G.; Hafner, J. *Phys. Rev. B: Condens. Matter Mater. Phys.* **1993**, *47*, 558.
(50) Perdew, J. P.; Burke, K.; Ernzerhof, M. *Phys. Rev. Lett.* **1996**, *77*, 3865.
(51) Heyd, J.; Scuseria, G. E.; Ernzerhof, M. *J. Chem. Phys.* **2006**, *124*, 219906.
(52) Gajdoš, M.; Hummer, K.; Kresse, G.; et al. *Phys. Rev. B: Condens. Matter Mater. Phys.* **2006**, *73*, 045112.
(53) Nosé, S. *J. Chem. Phys.* **1984**, *81*, 511.
(54) Hoover, W. G. *Phys. Rev. A: At., Mol., Opt. Phys.* **1985**, *31*, 1695.
(55) Barone, V.; Hod, O.; Scuseria, G. E. *Nano Lett.* **2006**, *6*, 2748−2754.
(56) Son, Y.-W.; Cohen, M. L.; Louie, S. G. *Phys. Rev. Lett.* **2006**, *97*, 216803.
(57) Kan, E.; Li, Z.; Yang, J.; Hou, J. G. *J. Am. Chem. Soc.* **2008**, *130*, 4224−4225.
(58) Li, X.; Wang, X.; Zhang, L.; Lee, S.; Dai, H. *Science* **2008**, *319*, 1229−1232.
(59) Jia, X.; Hofmann, M.; Meunier, V.; Sumpter, B. G.; Campos-Delgado, J.; Romo-Herrera, J. M.; Son, H.; Hsieh, Y.-P.; Reina, A.; Kong, J.; Terrones, M.; Dresselhaus, M. S. *Science* **2009**, *323*, 1701−1705.
(60) Park, C.-H.; Louie, S. G. *Nano Lett.* **2008**, *8*, 2200−2203.
(61) Topsakal, M.; Aktürk, E.; Ciraci, S. *Phys. Rev. B: Condens. Matter Mater. Phys.* **2009**, *79*, 115442.
(62) Mukherjee, R.; Bhowmick, S. *J. Chem. Theory Comput.* **2011**, *7*, 720−724.
(63) Raty, J.; Galli, G.; van Buuren, T.; et al. *Phys. Rev. Lett.* **2003**, *90*, 037401.
(64) Jiang, J.; Sun, L.; Gao, B.; Wu, Z.; Lu, W.; Yang, J.; Luo, Y. *J. Appl. Phys.* **2010**, *108*, 094303.
(65) Hu, W.; Li, Z.; Yang, J. *Comput. Theor. Chem.* **2013**, *1021*, 49.
(66) Zhang, J.; Zhang, M.; Sun, R.-Q.; Wang, X. *Angew. Chem., Int. Ed.* **2012**, *51*, 10145−10149.
(67) Ma, J.; Wang, L.-W. *Nano Lett.* **2015**, *15*, 248−253.
(68) Du, A.; Sanvito, S.; Li, Z.; Wang, D.; Jiao, Y.; Liao, T.; Sun, A.; Ng, Y. H.; Zhu, Z.; Amal, R.; Smith, S. C. *J. Am. Chem. Soc.* **2012**, *134*, 4393−4397.
(69) Qiu, D. Y.; da Jornada, F. H.; Louie, S. G. *Nano Lett.* **2017**, *17*, 4706−4712.
(70) Choi, J.-H.; Cui, P.; Lan, H.; Zhang, Z. *Phys. Rev. Lett.* **2015**, *115*, 066403.
(71) Bernardi, M.; Palummo, M.; Grossman, J. C. *ACS Nano* **2012**, *6*, 10082−10089.
(72) Xie, M.; Zhang, S.; Cai, B.; Huang, Y.; Zou, Y.; Guo, B.; Gu, Y.; Zeng, H. *Nano Energy* **2016**, *28*, 433−439.
(73) Zhou, L.-J.; Zhang, Y.-F.; Wu, L.-M. *Nano Lett.* **2013**, *13*, 5431−5436.
(74) Pham, T. A.; Ping, Y.; Galli, G. *Nat. Mater.* **2017**, *16*, 401−408.
(75) Ziletti, A.; Carvalho, A.; Campbell, D. K.; Coker, D. F.; Castro Neto, A. H. *Phys. Rev. Lett.* **2015**, *114*, 046801.
(76) Wang, G.; Slough, W. J.; Pandey, R.; Karna, S. P. *2D Mater.* **2016**, *3*, 025011.

DOI: 10.1021/jacs.7b08474
J. Am. Chem. Soc. 2017, 139, 15429−15436

(77) Wang, H.; Yang, X.; Shao, W.; Chen, S.; Xie, J.; Zhang, X.; Wang, J.; Xie, Y. *J. Am. Chem. Soc.* **2015**, *137*, 11376−11382.
(78) Pei, J.; Gai, X.; Yang, J.; Wang, X.; Yu, Z.; Choi, D.-Y.; Luther-Davies, B.; Lu, Y. *Nat. Commun.* **2016**, *7*, 10450.
(79) Ran, J.; Gao, G.; Li, F.-T.; Ma, T.-Y.; Du, A.; Qiao, S.-Z. *Nat. Commun.* **2017**, *8*, 13907.

DOI: 10.1021/jacs.7b08474
J. Am. Chem. Soc. 2017, 139, 15429−15436